Optics & Laser Technology 51 (2013) 36–42

Contents lists available at SciVerse ScienceDirect

Optics & Laser Technology

journal homepage: www.elsevier.com/locate/optlastec

UV laser induced selective-area bandgap engineering for fabrication of InGaAsP/InP laser devices

Mohammad Kaleem [a,*], Xin Zhang [a], Yuan Zhuang [a], Jian-Jun He [a], Neng Liu [b], Jan J. Dubowski [b]

[a] State Key Laboratory of Modern Optical Instrumentation, Department of Optical Engineering, Zhejiang University, Hangzhou 310027, China
[b] Laboratory for Quantum Semiconductors and Photon-based BioNanotechnology, Interdisciplinary Institute for Technological Information (3IT), Université de Sherbrooke, Sherbrooke, Québec, Canada J1K 2R1

ARTICLE INFO

Article history:
Received 21 November 2012
Received in revised form
12 March 2013
Accepted 16 March 2013
Available online 21 April 2013

Keywords:
Quantum well intermixing
Photonic integration
Semiconductor laser

ABSTRACT

Large bandgap blueshifts in III–V quantum semiconductor microstructures are achievable with UV-laser induced quantum well intermixing (QWI). We report on the application of the UV-laser QWI technique to investigate bandgap engineering of a compressively strained InGaAsP/InP quantum well laser microstructure. The attractive performance of the technique, determined by the ability of a laser to generate point defects, has been demonstrated with bandgap blueshifts reaching 142 nm, with enhancement of photoluminescence intensity. We have also investigated this technique for post-growth wafer level processing designed for the fabrication of laser diodes.

1. Introduction

Integrated optics promises components which will extend the bandwidth and/or switching capabilities of fiber optics communications and provides very rapid information processing between active devices interconnected through low loss waveguides. Integration of devices offers significant improvements in mechanical stability and reliability, as well as device miniaturization [1]. The realization of photonic integrated circuits (PICs) requires spatially selective control over the local optical and electrical characteristics of the multiple quantum well (MQW) material. Many monolithic fabrication techniques have been developed. Selective regrowth and selective area epitaxy are two promising techniques. However, the regrowth techniques require expensive facilities such as metal–organic vapor phase epitaxy (MOVPE) during the fabrication process and yields are usually low. Selective area epitaxy using silica masking allows regions with different bandgaps to be realized across a wafer in a single growth step, but such an approach does not allow complete control of the bandgap in two dimensions [1]. Post growth quantum well intermixing (QWI) is an attractive alternative method to engineer the bandgap of quantum well (QW) semiconductors in which the absorption edge is permanently changed by intermixing the wells and barriers.

Numerous QWI techniques have been developed in the past decades, such as impurity-induced disordering (IID), impurity-free vacancy disordering (IFVD) [1,2], ion implantation induced disordering (IIID) [3,4], argon plasma induced disordering [5] and plasma induced damage during the deposition of sputtered SiO_2 [6]. UV-laser induced disordering (UVLID) QWI technique is one of the promising methods reported in the literature [7–13]. In this technique, point defects are created near the surface of quantum well (QW) chip by UV-laser irradiation, and the diffusion of these point defects downward to the QW region in the rapid thermal annealing (RTA) process leads to large bandgap energy shifts. A top sacrificial layer of InP (e.g. 500 nm thick) is commonly used to serve as a reservoir for laser generated point defects. The exchange of group V species e.g., P and As, and group III species, e.g., Ga and In causes change of potential barrier height and the well width. This leads to blueshifts of the optical absorption edge and formation of a different bandgap QW material. This post-growth wafer level fabrication of multibandgap QW material facilitates active and passive components to be integrated monolithically at relatively reduced costs.

It is known that the absorption of UV-laser radiation by solids can induce disruption to the lattice and lead to the intermixing effect. The bond strength of InP is lower than the bond strength of InGaAs [13]. Thus, by using an InP top sacrificial layer we can achieve higher concentration of point defects with even low UV-laser fluences in the sacrificial layer while the InGaAs surface remains undamaged which is necessary for the fabrication of photonic devices on the QWI altered material. The resulting material can have high optical and electrical quality.

Previous published work [8,12,13] demonstrated blueshifts up to 130 nm using unstrained InGaAs/InGaAsP QW laser structure. In this paper we report superior experimental results with wavelength blueshifts as large as 142 nm in compressively strained InGaAsP/InP QW laser structure using the combination of UV-laser irradiation process and rapid thermal annealing treatment. We show that the

* Corresponding author. Tel.: +86 131 736 55579.
E-mail address: kaleemmuk@yahoo.co.uk (M. Kaleem).

0030-3992/$ - see front matter © 2013 Elsevier Ltd. All rights reserved.
http://dx.doi.org/10.1016/j.optlastec.2013.03.012

photoluminescence (PL) intensity can be enhanced with reduced linewidth under certain UV irradiation conditions, possibly due to the change of strain distribution in the QW that alters the band structure and enhances the Fermi occupation factor. By using a thick InP sacrificial layer that is removed after UV irradiation and RTA, little surface damage was observed which might affect the device performance. Preliminary results on the application of the UV-laser QWI technique for laser device fabrication are also presented.

2. UV laser QWI in InGaAsP/InP microstructures

The investigated sample of InGaAsP/InP laser structure contains five 1% compressively strained $In_{0.8}Ga_{0.2}As_{0.8}P_{0.2}$ QWs with unstrained 1.25Q InGaAsP barriers. From the surface the layers are a 0.5 μm Zn-doped (10^{18} cm^{-3}) InP sacrificial layer, 0.2 μm Zn-doped (10^{19} cm^{-3}) $In_{0.53}Ga_{0.47}As$ cap, 1.5 μm Zn-doped (10^{18} cm^{-3}) InP cladding, 0.004 μm Zn-doped (4×10^{17} cm^{-3}) 1.3Q InGaAsP etch-stop layer, 0.15 μm Zn-doped (4×10^{17} cm^{-3}) InP cladding, five repeats of 10 nm undoped InGaAsP barrier (λ_g=1.25 μm) and 5.5 nm undoped $In_{0.8}Ga_{0.2}As_{0.8}P_{0.2}$ QW which are sandwiched by two 0.06 μm InGaAsP step-graded index separate confinement layers with the bandgap wavelength λ_g varying from 1.05 μm to 1.25 μm, and 1.5 μm Si-doped (2×10^{18} cm^{-3}) InP buffer on Si-doped (4×10^{18} cm^{-3}) InP substrate.

A fragment of the InGaAsP/InP wafer was irradiated with a KrF laser (ProMaster OPTEC, ATLEX 300i, λ=248 nm) delivering 22 ns pulses of fluence in the range of 50–200 mJ/cm^2. The sample was irradiated at room temperature and at normal incidence to the surface. The pulse repetition rate was 10 Hz. The laser beam was not homogenized and the spots of almost rectangular shape were created on the sample surface without using a mask. The *X*–*Y*–*Z* positioning of the sample was controlled by a computer. This UV-laser setup allowed for the processing of the same sample at numerous sites, each measuring approximately 600×500 μm^2. After being exposed to the laser, the samples were annealed in a nitrogen atmosphere using an RTA furnace operating at 750 °C for 120 s. During the RTA processing, samples were placed between two Si wafers to prevent desorption of the group V elements. Since numerous sites of the same sample could be processed with different laser parameters, the annealing conditions were the same for different spot sites. The possible damage generated during the UV-laser process was investigated before and after RTA treatment.

The bandgap shifts induced by the above UV-laser procedure were measured using room temperature photoluminescence (PL) measurements. The photoluminescence mapper using a Nd:YAG (yttrium aluminum garnet) laser (λ=1064 nm) was used as an excitation source along with a photo-detector array built in a spectrum analyzer. The under observation sample was placed on a computer-controlled *x*–*y* stage, which was moved in 17.5 μm steps. With the computer software collecting data as a function of the *x*–*y* position, a two dimensional map for the peak wavelength and intensity was measured. For each spot, we first measured the wavelength at the peak position of the UV-laser beam profile and then looked at the corresponding intensity of the same point in the same spot. This procedure is repeated for each spot. The PL spectral peak corresponds to the QW electron–hole recombination peak, which for the as-grown material is obtained at 1553 nm.

Prior to the QW intermixing, we take a thermal stability test with the as-grown sample to determine the blueshift induced by the RTA-only process. The InGaAsP/InP MQW laser sample exhibits bandgap shifts at temperatures as low as 660 °C. The bandgap shift increases rapidly with increasing anneal temperature. The observed bandgap blueshift for RTA-only sample is about 23 nm at 750 °C. It goes up to 30 nm at temperatures above 770 °C. The PL intensity tends to decrease and the peak broadening is observed after the RTA treatment. The thermal interdiffusion is believed to be responsible for the change of the confinement profile and strain distribution in the MQW structure. Furthermore, it is possible that the diffusion of both the dopants (Zn) and surface chemical defects also contributed to the decrease of PL intensity.

Fig. 1 shows the wavelength and intensity map of the PL spectra for QW sample after the combination of UV-laser irradiation and RTA procedures. The PL maps were measured after removing the sacrificial layer and the InGaAs cap layer. For clarity, each spot site of each row is marked with letters and the corresponding data is presented in Table 1. It can be seen clearly that a noticeable large blueshift is achieved with even 50 pulses of UV-laser irradiation. The formation of an array of clearly distinguishable sites of multiple bandgap material took place following the combination of UV-laser irradiation and RTA treatment. Spots were not uniform due to the fact that the UV-laser beam used in this experiment was not uniform.

Table 1 gives the detailed information about the laser irradiation conditions, the achieved blueshifts, the peak PL intensity and the full width at half maximum (FWHM) for each spot shown in Fig. 1. The first three spots (A1–A3) in the first row exhibit wavelength shift of nearly 100 nm. The wavelength shift of about 122 nm is achieved in the 2nd row 1st column spot (A4) of the sample. Similarly, even larger wavelength shift is achieved in the 4th row and onwards which suggests that wavelength shift tends to increase as the UV-laser energy and number of pulse doses increase. The wavelength blueshift is more uniform at greater number of pulses. However, we observe that at maximum wavelength shift, the intensity is slightly reduced. Fig. 1b presents the intensity map of the same sample after UV-laser processing and RTA treatment. The peak intensity of the as-grown sample is 1.92 nW while its linewidth (FWHM) is 93.4 nm. For the RTA-only region, the peak intensity decreases to 1.7 nW while the linewidth is increased to 109 nm. The intensity of the first three spots A1–A3 in the 1st row of the sample is about 2.3–2.7 nW which is much higher than that of the as grown sample as well as the RTA-only region. The linewidth ranges from 75.7 to 80.6 nm, which is also much narrower. Similarly, the 2nd row intensity of all five spots (A4 and B1–B4) is between 2.0 and 2.7 nW which is again much higher and narrower than that of the as grown sample and RTA-only region. Since two spots in the 2nd row overlapped they were repeated in the last row marked as A4* and B1*. On average, almost all the rest of the spots exhibit intensity higher than that of the as grown sample and the RTA-only region. We did not use extended parameters of UV-laser energy and the number of pulses knowing that it would lead to the saturation of the wavelength shift and can damage the InGaAs surface which can degrade the performance of photonic devices [11,12]. The compressively strained InGaAsP/InP QW laser structure used here is different from unstrained QW structure in previously reported work [8,13]. The structure used in this experiment also has a thicker sacrificial layer of 500 nm (Zn-doped), and thus a larger reservoir for generating large number of point defects. By using a thick InP sacrificial layer which is removed after UV irradiation and RTA, little surface damage was observed which may affect the device performance.

Examples of 3D PL wavelength and intensity maps have been shown in Figs. 2 and 3 for A1 and B1′ spots, respectively. We can see that most of the PL emission from these spots is located near 1.46–1.47 μm. However, fragments of the central portion of those spots emit at a less blueshifted wavelength of ~1.51 μm. For instance, the maximum and minimum PL intensity of the A1 spot illustrated in Fig. 3b is, respectively, about 2.7 nW and 0.8 nW. This non-uniform distribution of the blueshift amplitude and the intensity within the spot is a finger print of the non-uniform

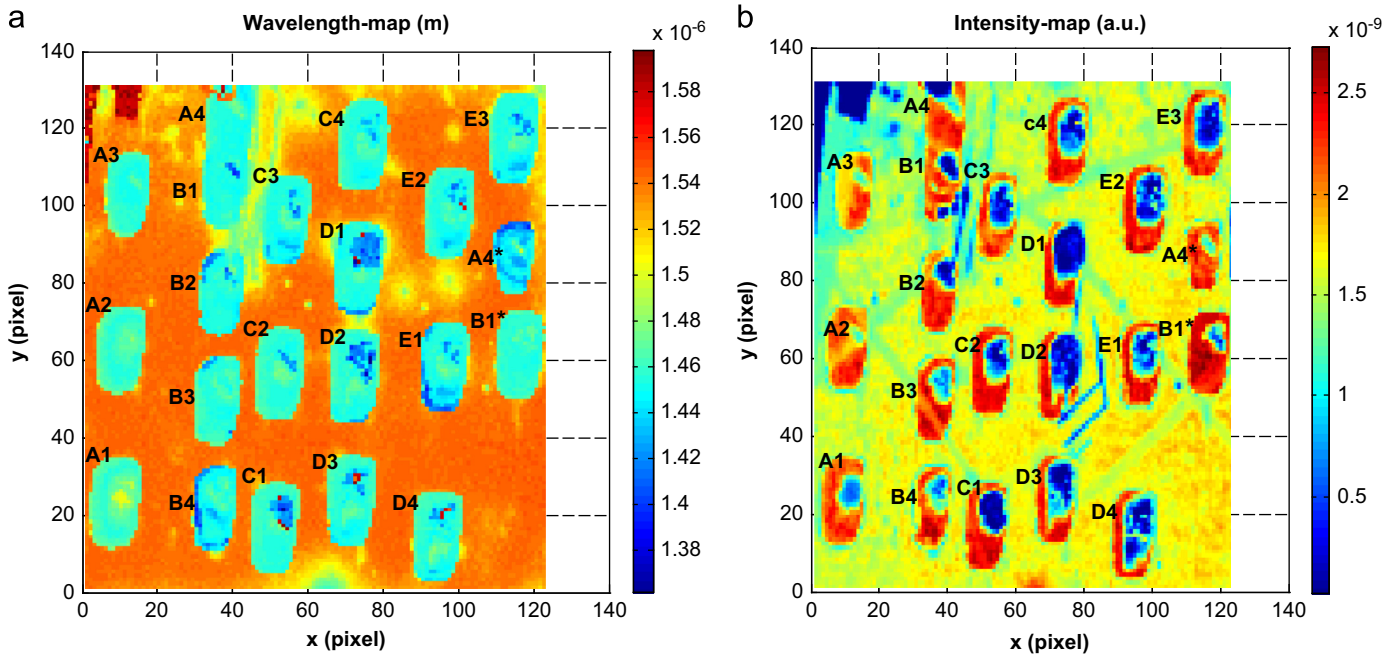

Fig. 1. Room temperature PL wavelength (a) and intensity (b) maps of a KrF laser processed InGaAsP/InP MQW sample after rapid thermal annealed at 750 °C for 120 s.

Table 1
Processing parameters and PL results.

Spot	No. of pulses	Pulse energy (mJ/cm^2)	Blueshift (nm)	Intensity (nW)	FWHM (nm)
As-grown	0	0	0	1.92	93.4
RTA-only	0	0	23	1.7	109
A1	50	50	98	2.7	80.6
A2	100	50	103	2.3	77.6
A3	150	50	102	2.3	75.7
A4	200	50	122	2.6	84
B1	50	100	103	2.7	79.8
B2	100	100	123	2.6	90.7
B3	150	100	102	2.2	81
B4	200	100	112	2.0	78.7
C1	50	150	101	2.8	79.1
C2	100	150	102	2.1	78.3
C3	150	150	105	2.0	77.2
C4	200	150	125	2.1	93
D1	50	200	103	2.3	78.3
D2	100	200	130	1.9	93.8
D3	150	200	107	2.0	75.3
D4	200	200	103	2.0	85.8
E1	140	160	107	2.4	81
E2	160	160	102	2.4	78.7
E3	180	160	98	1.9	84
A4*	200	50	125	2.1	90.7
B1*	50	100	103	2.6	75.7

distribution of the laser beam applied in this experiment. However, we note that both wavelength and intensity maps of the B1′ spot (Fig. 3) that were produced with twice the pulse energy ($E=100$ mJ/cm^2) compared to that used to produce the A1 spot, are more uniform than those of the A1 spot (Fig. 2).

The above phenomenon can be explained by the saturation of the blueshift amplitude observed for the relatively increased pulse fluence that was observed for the similar QW microstructure [8,12]. In the case investigated here, the QWI effect was induced with the laser pulse energy increased from 50 mJ/cm^2 (A1) to 100 mJ/cm^2 (B1′). This has allowed fabricating a site with a more uniformly emitted PL signal due to the excimer laser operating in the blueshift plateau regime. Fig. 3b shows that the PL intensity, in the most part of the site is at about 2.6 nW, while at the center of the excimer laser induced intensity dip, the emission power is at near 0.9 nW. The non-uniformity of the laser beam profile in this 1st experiment is the main reason and, an addition of homogenizer is a solution and was used in the 2nd experiment described in Section 3.

The net blueshift listed in Table 1 was calculated by taking into account that, following the RTA step, the PL emission wavelength of the non-irradiated QW microstructure was blueshifted by 23 nm. The interesting observation is that most of the blueshift amplitude is achieved with the first 50 laser pulses. The further increase of the laser irradiation dose has resulted in a minor increase only of the blueshift amplitude. Furthermore, for the 200 mJ/cm^2 irradiated sites, the greatest laser fluence applied in this experiment, the blueshifts obtained for the 50 and 200-pulse irradiated sites are essentially the same (compare D1 and D4 sites). At certain UV-laser energy density parameters, the PL intensity becomes higher while in other part of the spot, it goes down. When energy is too high, it produces too many defects but for certain energy density it produces large amount of intermixing while the defects are insignificant.

A systematically strong PL emission has been observed for all the laser processed sites. For comparison, the interesting feature of the applied QWI method is that the intensity tends to increase in all cases as the sample undergoes UV-laser processing and RTA treatment. The intensity of all spots increases instantly and in some cases becomes almost 3 nW which is much higher than that of the as grown sample while a blueshift of about 100 nm is quite noticeable using only 50 pulses of UV-laser irradiation. Fig. 4 shows PL spectra of selected spots, following UV-laser irradiation and RTA treatment. It can be seen that the differential shift between the RTA-only sample and the disordered sample that was processed with the combination of the UV-laser irradiation and RTA is over 100 nm. It can also be seen that not only the peaks have been shifted well over 100 nm relative to the sample which is not irradiated, but also the intensities of the under observation spots have also increased significantly with a reduction of the linewidth. The narrowing of the PL linewidth indicates that the

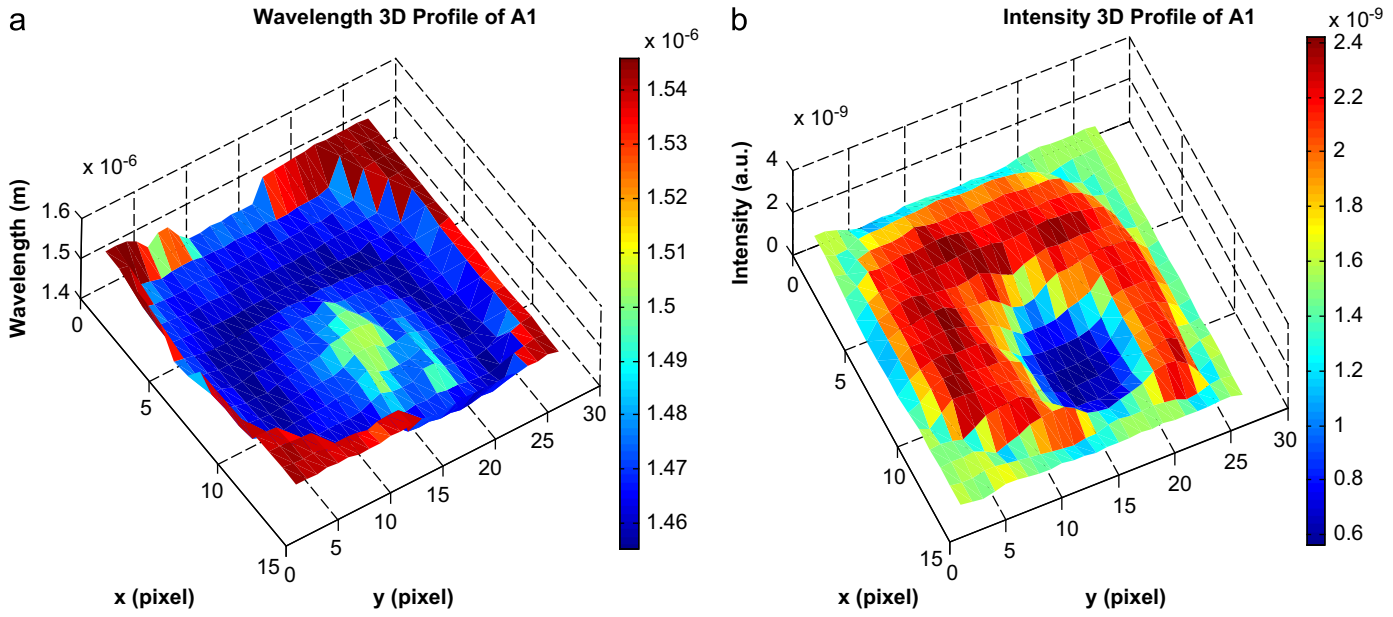

Fig. 2. Wavelength and intensity 3D PL maps of the A1 spot on the InGaAsP/InP sample irradiated with the UV laser at 50 mJ/cm^2 and RTA at 750 °C for 2 min.

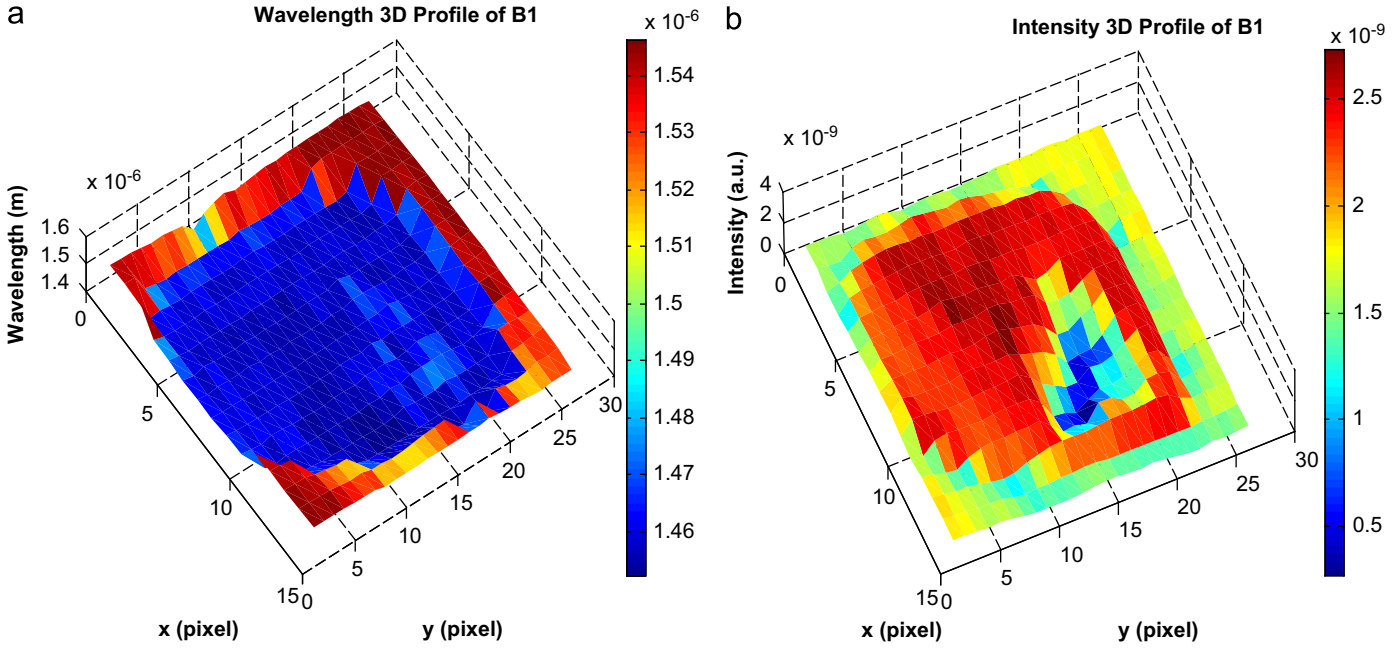

Fig. 3. Wavelength and intensity 3D PL maps of the B1′ spot on the InGaAsP/InP sample irradiated with the UV-laser at 100 mJ/cm^2 and RTA at 750 °C for 2 min.

intensity enhancement in this experiment is due to change of QWs rather than any surface effect as reported in earlier work [11,13].

The large PL wavelength shift and intensity enhancement at certain UV irradiation conditions can be attributed to the intermixing induced quantum well shape rounding and the change of strain distribution in the QW that alters the band structure and enhances the Fermi occupation factor. Using the expanded form of Fick's second law, Chan et al. [14] calculated the band structure and optical gain of intermixed $In_{0.53}Ga_{0.47}As/In_{0.52}Al_{0.48}As$ quantum well and found that the optical gain can be enhanced by 40% compared to as-grown material, due to an improvement of the Fermi occupation factor resulted from change in the splitting between the heavy and light holes. The optical gain first increases with the degree of intermixing and then decreases as the intermixing reaches a certain degree. Although the detailed theoretical simulation is to be performed, it is reasonable to believe that a similar mechanism can explain the observed PL intensity enhancement and linewidth narrowing in the QWI material. The PL intensity is enhanced at certain degree of intermixing, corresponding to a certain energy density of the UV irradiation. As the degree of intermixing increases, the PL intensity first increases and then decreases. It is therefore possible to produce a PL intensity dip in the middle of the UV irradiation spot.

The above PL spectra prove that laser-induced point defects generated during the UV-laser irradiation step and RTA can lead to the fabrication of high-quality QWI material. The process enables relatively large bandgap shift to be obtained on a single wafer of an InGaAsP/InP laser structure. Such bandgap shifts are attractive for the fabrication of monolithically integrated active–passive devices. In the following section we present our preliminary results on the use of UV irradiation with an aluminum mask for

the laser device fabrication with selective regions of the QWI material.

3. UV laser QWI for laser device fabrication

In order to investigate advantage of the UV-laser QWI technique, a dedicated sample was coated with a 70 nm thick Al mask with arrays of 40 μm × 200 μm rectangular windows. The mask, whose pattern was originally designed for 16 × 100 GHz digitally wavelength-switchable V-coupled-cavity laser diodes [15], was fabricated using a standard laser fabrication process which contains etched facet fabrication, waveguide fabrication and then electrode deposition.

The sample was irradiated in a KrF laser (Lumonics, Pulse Master 800) processing station equipped with a double micro-lens fly-eye-array beam homogenizer [12]. A rectangular mask of 40 mm × 4 mm was used in this case at a demagnification ratio of 1.8. The irradiation was carried out in an air environment with 200 pulses, each delivering a fluence of 156 mJ/cm^2. A computer controlled *X*–*Y*–*Z*–Theta sample holding stage allowed for processing relatively large regions of the wafer by applying a step-and-repeat technique. Following the laser irradiation step, the Al film was removed by exposing the sample for 5 min in a diluted 2.5% Tetramethylammonium hydroxide (TMAH; Sigma-Aldrich, Canada) solution. The cleaned sample was annealed for 2 min at 700 °C in an atmosphere of mixed hydrogen and nitrogen forming gas (N_2:H_2 = 1:9) of a rapid thermal annealing (RTA) furnace (JIPELEC, Jetfirst). A relatively low annealing temperature (700 °C) was used to minimize the bandgap shifting in the non-irradiated material to near 15 nm.

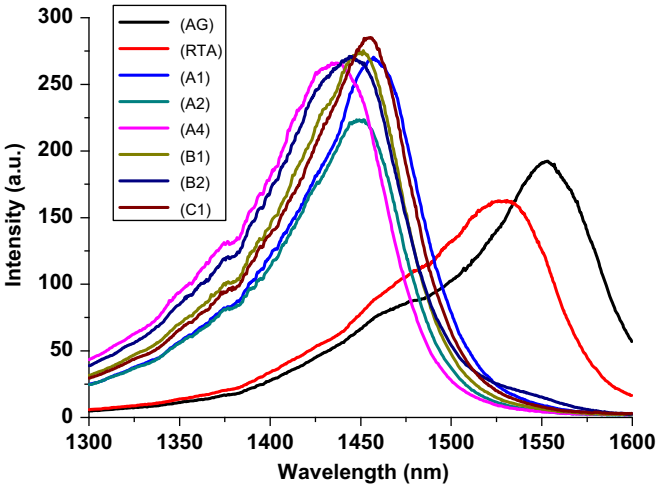

Fig. 4. Comparison of photoluminescence (PL) shifts for InGaAsP/InP samples under gone through different treatments such as only RTA and UV-laser plus RTA at temperature 750 °C with as-grown (AG) sample.

A commercial PL mapper (Philips PLM 150) was employed in this case for collecting maps of processed samples. The measurements were carried out by collecting PL signal averaged over 160 μm, dispersed by a monochromator and detected by an InGaAs photodiode array.

Fig. 5 (left panel) shows the PL map of a fragment of the InGaAs/InP QW sample irradiated with the KrF setup (Lumonics, Pulse Master 800) and annealed in the RTA furnace. An array of sites, approximately 40 μm × 200 μm, can be seen in this case. The top-left graph shows an expanded view of the PL map of three mask windows, showing good uniformity within the windows. Here, we use the scanning step at 10 μm in the short side (~40 μm) direction (horizontal) and 20 μm in the long side (~200 μm) direction (vertical). A cross-sectional scan covering a region with 8 blue-shifted windows, shown in the right panel of Fig. 5, provides more details of the processed microstructure. A uniform emission at near 1442 nm is observed from each window, while the background emits at 1515 nm. The net 73 nm blueshift achieved in this case is a promising result toward the fabrication of enhanced performance wavelength-switchable V-coupled-cavity laser diodes or other devices taking advantage of the multibandgap wafers.

In order to investigate the properties of the UV-laser QWI material for photonic device fabrication, Fabry–Perot (FP) laser diodes were fabricated on a piece of wafer with one half of the piece undergoing the QWI process and the other half undergoing RTA only for comparison. The QWI region was irradiated with 50 pulses of KrF laser of fluence 50 mJ/cm^2 at the pulse repetition rate of 10 Hz. Since the irradiation window of the setup was only about 600 × 500 μm^2 with lower intensity at the edges, the QWI region was obtained by using a step-and-repeat process, with step sizes

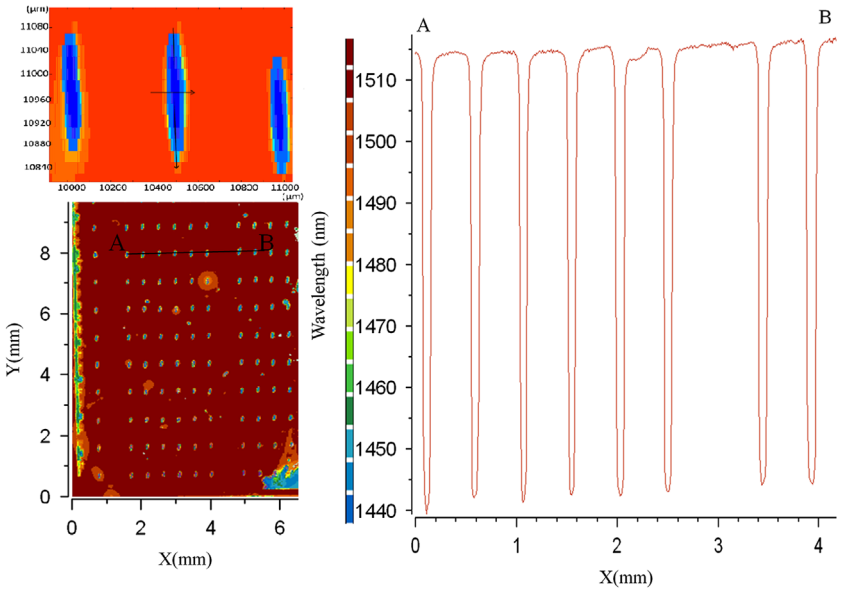

Fig. 5. PL map (left) and PL scanning profile (right), line from A to B, of InGaAs/InP QW microstructure after KrF laser irradiation at 156 mJ/cm^2 with 200 pulses through Al film mask with 40 μm × 200 μm windows and RTA at 700 °C for 2 min. The top-left graph shows an expanded view of the PL map of the mask windows.

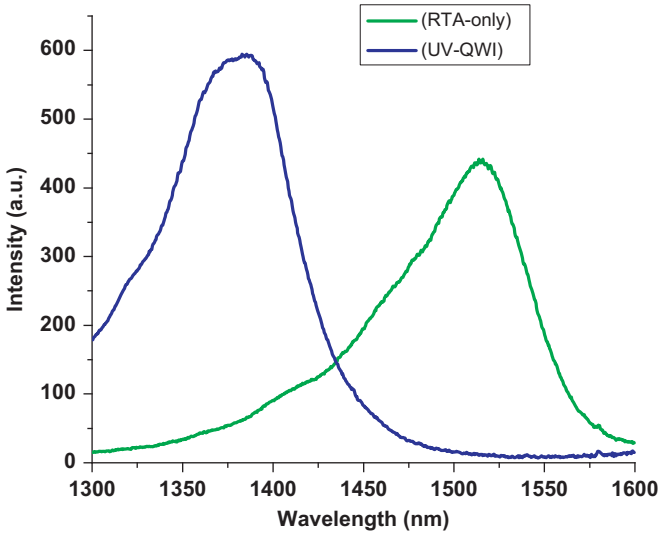

Fig. 6. Comparison of photoluminescence spectra for InGaAsP/InP samples through different treatments of UV-irradiation plus RTA (QWI) and RTA-only at temperature 750 °C.

of 300 μm and 250 μm in the *X* and *Y* directions, smaller than the window size to improve the uniformity. After being exposed to the laser, the sample was annealed in a nitrogen atmosphere using the RTA furnace operating at 750 °C for 120 s. Fig. 6 shows the PL spectra of UV-laser QWI region and the RTA-only region. The PL peak shifted from 1525 nm in the RTA-only region to 1383 nm in the QWI region, with a net blueshift of 142 nm. The peak intensity is increased by 34%. The FWHM of the UV-laser QWI curve is measured to be 87 nm while that of the RTA-only region is about 90 nm.

After the QWI process, standard Fabry–Perot laser structure was fabricated. The length of the fabricated lasers is 500 μm, with ridge waveguide of 3 μm wide. Fig. 7 shows the *L–I* characteristics of the FP lasers from the UV-QWI region and from the RTA-only region. The UV-QWI processed laser has threshold current of 28 mA which is lower than that of the RTA-only laser at 36 mA. This is consistent with the results of the PL intensities. Fig. 8 shows the emission spectra of the UV-QWI laser and the RTA-only laser. The emission peak of the QWI laser has been blueshifted from 1535 nm to 1405 nm, with a net blueshift of 130 nm, while the profile of the laser spectrum remains essentially the same. This further confirms that under appropriate conditions this QWI technique does not affect the lasing property of the material while achieving a large blueshift.

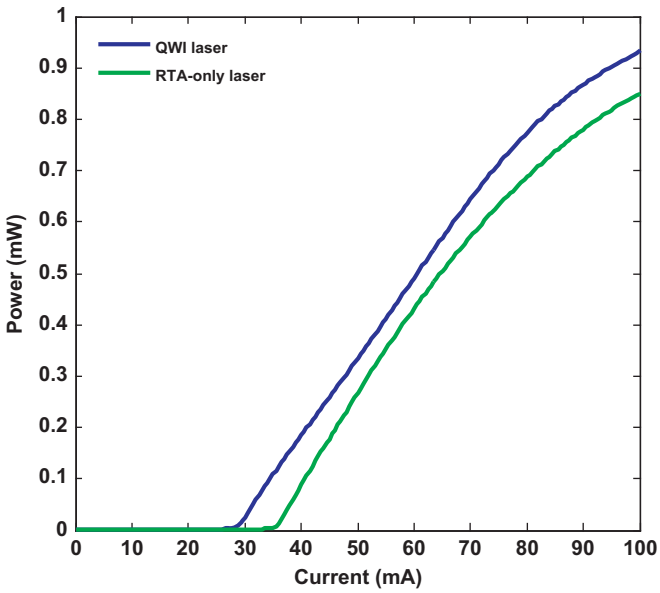

Fig. 7. *L–I* characteristics of the UV-QWI laser and the RTA-only laser.

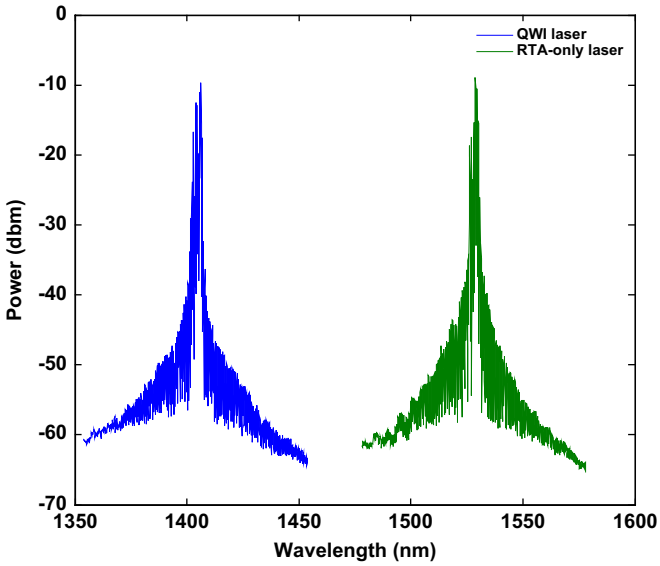

Fig. 8. Laser spectra of the UV-QWI laser and the RTA-only laser.

4. Conclusions

We have employed the UV-laser QWI technique to investigate bandgap engineering of compressively strained InGaAsP/InP QW laser microstructures. The application of a simple excimer laser setup allowed achieving net blueshifts as large as 142 nm in the investigated material. One of the attractive features of this approach is that the photoluminescence intensity of the laser processed material can be enhanced, and there is a negligible presence of defects responsible for deterioration of the photonic properties of the material. The irradiation with 200 pulses of a homogenized beam laser, followed by RTA at 700 °C, produced an array of 73 nm blueshifted windows (40 μm × 200 μm) of the material attractive for the fabrication of a laser with multiple bandgaps for advanced functionalities. Fabry–Perot laser diodes have also been fabricated and a lower threshold current is measured for the QWI laser as compared to that of RTA-only laser, while the wavelength is blueshifted by about 130 nm with similar profiles of the emission spectra. The experimental results have demonstrated the potential of the UV laser QWI technique for the fabrication of integrated multibandgap photonic devices.

Acknowledgments

This work is supported by the Ministry of Science and Technology of China under international collaborative research (Grant no. 2010DFA61370), the Natural Science Foundation of Zhejiang Province (Grant no. Z1110276), the National High-Tech R&D Program of China (Grant no. 2013AA014401) and the Canada Research Chair in Quantum Semiconductors Program.

References

[1] Marsh JH, Kowalski OP, MacDougall SD, Qiu BC, McKee A, Hamilton CJ, et al. Quantum well intermixing in material systems for 1.5 μm. Journal of Vacuum Science and Technology A 1998;16:810.

[2] Marsh JH. Quantum well intermixing. Semiconductor Science and Technology 1993;8:1136–55.
[3] Charbonneau S, Koteles ES, Poole PJ, He J-J, Aers GC, Haysom JE, et al. Photonic integrated circuits fabricated using ion implantation. IEEE Journal of Selected Topics in Quantum Electronics 1998;4:772–93.
[4] He J-J, Feng Y, Koteles ES, Poole JP, Davis M, Dion M, et al. Bandgap shifted InGaAsP/InP quantum well waveguides using MeV ion implantation. Electronics Letters 1995;31:2094–5.
[5] X. Zhang, J.-J. He, Optical loss of bandgap shifted InGaAsP/InP waveguide using argon plasma-enhanced quantum well intermixing, Advances in Optoelectronics and Micro/Nano-Optics (AOM), 2010 OSA-IEEE-COS, 1-2.
[6] Kowalski OP, Hamilton CJ, McDougall SD, Marsh JH, Bryce AC, De La Rue RM, et al. Universal damage induced technique for quantum well intermixing. Applied Physics Letters 1998;72:581–3.
[7] Genest J, Dubowski JJ, Aimez V, Pauc N, Drouin D, Post M. UV laser controlled quantum well intermixing in InAlGaAs/GaAs heterostructures. Journal of Physics: Conference Series 2007;59:605–9.
[8] Liu N, Moumanis K, Dubowski JJ. Surface morphology of SiO_2 coated InP/InGaAs/InGaAsP microstructures following the irradiation with ArF and KrF excimer laser. Proceedings of SPIE 2010;7920 79200C1-11.
[9] Qiu BC, Bryce AC, De La Rue RM, Marsh JH. Monolithic integration in InGaAs–InGaAsP multiquantum-well structure using laser processing. IEEE Photonics Technology Letters 1998;10:769–71.
[10] Dubowski JJ, Poole PJ, Sproule GI, Marshall G, Moisa S, Lacelle C, et al. Enhanced quantum-well photoluminescence in InGaAs/InGaAsP heterostructures following excimer-laser-assisted surface processing. Applied Physics A 1999;69(Suppl.):S299–303.
[11] Liu N, Moumanis K, Blais S, Dubowski JJ. XPS study of InP/InGaAs/InGaP microstructures irradiated with ArF laser in air and deionized water. Proceedings of SPIE 2012;8245:82450E1–12.
[12] Liu N, Dubowski JJ. Chemical evolution of InP/InGaAs/InGaAsP microstructures irradiated in air and deionized water with ArF and KrF lasers. Applied Surface Science 2013;270:16–24. http://dx.doi.org/10.1016/j.apsusc.2012.12.007.
[13] Genest J, Beal R, Aimez V, Dubowski JJ. ArF laser-based quantum well intermixing in InGaAs/InGaAsP heterostructures. Applied Physics Letters 2008;93:071106.
[14] Chan Y, Chan Michael CY, Herbert Li E. Three-cation intermixed InGaAs/InAlAs quantum well structures and their optical gain properties. Proceedings of SPIE 1998;3283:357–64 Physics and Simulation of Optoelectronic Devices VI.
[15] Jin J, Wang L, Wang Y, Yu T, He J-J. Widely wavelength switchable V-coupled cavity semiconductor laser with 40 dB side-mode suppression ratio. Chinese Optics Letters 2011;36:4230–2.